Japanese Journal of Applied Physics

The Japan Society of Applied Physics

REGULAR PAPER • OPEN ACCESS

Great enhancement of sensitivity for SARS-CoV-2 detection by integrated graphene FET biosensor using ζ potential modulator

OPEN ACCESS

Japanese Journal of Applied Physics **63**, 03SP14 (2024) **REGULAR PAPER**

https://doi.org/**10.35848/1347-4065/ad1e99**

Great enhancement of sensitivity for SARS-CoV-2 detection by integrated graphene FET biosensor using ζ potential modulator

Kaori Yamamoto[1*], Natsuki Sato[1], Kiyoji Sakano[1], Mamiko Yano[1], Eriko Ohnishi[1], Takao Ono[1], Yasushi Kanai[1], Shota Ushiba[2], Naruto Miyakawa[2], Shinsuke Tani[2], Masahiko Kimura[2], Yohei Watanabe[3], Koichi Inoue[1], Hidekazu Tanaka[1], and Kazuhiko Matsumoto[1]

[1]*Osaka University, Ibaraki, Osaka 567-0047, Japan*
[2]*Murata Manufacturing Co., Ltd., 1-10-1 Higashikotari, Nagaokakyo-shi, Kyoto 617-8555, Japan*
[3]*Kyoto Prefecture University of Medicine, Kajii-cho, Kamigyo-ku, Kyoto-shi, Kyoto 602-8566, Japan*

[*]E-mail: k-yamamoto@sanken.osaka-u.ac.jp

Received October 13, 2023; revised December 25, 2023; accepted January 14, 2024; published online February 12, 2024

By modulating a ζ potential of graphene FET (G-EFT), the sensitivity of G-FET could be enhanced than that without modulation. Therefore, 1×10^7 FFU ml^{-1} SARS-CoV-2 was detected using G-FET modified with the ζ potential modulator which is the cation polymer with the positive charge. This method is based on the relationship between the surface charge and the sensitivity, in which the highest sensitivity is obtained when the ζ potential is 0 and/or the surface charge is almost 0. In this study, the microfluidic channel was installed on G-FET to get the precise result because it could wash away the free-floating virus and the physical adsorbed virus. 32 G-FETs including the reference FETs were integrated on the silicon substrate and the precise results were obtained by subtracting the noise terms.

1. Introduction

Graphene is well known to have various features such as a high mobility of ∼200 000 cm^2 Vs^{-1}, two-dimensional electron gas is on its surface, etc. Also, graphene is stable even in the solution, and is easy to be modified by various receptor.[1–4] By using these advantages, we have been developing G-FET biosensor in order to detect the various viruses and proteins, etc.[5–13]

In this study, the ζ potential modulator which is poly-L-lysine (PLL) was introduced into G-FET to enhance the sensitivity.[14] To get the optimum PLL concentration, G-FET modified with the different concentrations of PLL was used to detect SARS-CoV-2. PLL concentration was changed from 0.5 ng ml^{-1} to 5 mg ml^{-1}. As a result, maximum Dirac point shift was obtained when G-FET was modified with 50 μg ml^{-1} PLL. Thus, 50 μg ml^{-1} PLL was used all through this study. The top gate voltage V_G at the minimum drain current I_D is known as the charge neutrality point or Dirac point.[15] When the ζ potential on the graphene surface is almost 0, G-FET shows the highest sensitivity.[16,17] Owing to the spontaneously induced negative charge on the graphene surface, however, it is said that G-FET have the negative ζ potential of ∼45 mV[18] and it is difficult to get the higher sensitivity as it is. In order to get the higher sensitivity, we introduced the ζ potential modulator with the positive charge which can cancel out the negative charge of the graphene surface. This effect reduces the ζ potential near to 0. In addition, we installed the microfluidic channel onto G-FETs to remove the physical adsorption of the virus and the virus not bound to the antibody in the solution. Using the microfluidic channel, quantitative washing becomes possible. And the reliability of the average and the standard deviation of the Dirac point becomes increased compared to the conventional manual pipetting process.[19] In the present paper, G-FETs modified with and without the ζ potential modulator were fabricated on the same substrate. G-FET without the ζ potential modulator were used as reference FETs. The enhancement of the sensitivity by the ζ potential modulator was confirmed precisely. And 10^7 FFU ml^{-1} SARS-CoV-2 in 1 × PBS could be detected by G-FET. This viral concentration is almost the same as that in the saliva of a human infected with SARS-CoV-2. Thus, G-FET has a possibility to detect the whole SARS-CoV-2 virus directly from the saliva. In most previous studies, the spike protein,[20–22] the nucleocapsid protein[22] and RNA[23] from SARS-CoV-2 were detected, but only few studies show to detect whole viruses. Compared with these previous methods which should take out these proteins and RNA, G-FET in the present study have the advantages of fast detection and easy operation because whole viruses could be detected directly by G-FET.

2. Experimental methods

We have been studying to detect SARS-CoV-2 using integrated G-FET with high sensitivity. Figure 1(a) shows the optical image of the integrated 32 G-FETs, and (b) the expanded view of one G-FET. G-FET has an inter digital structure and the channel length and the width were 10 μm and 400 μm, respectively. The graphene layer was put onto the Ti/Au source/drain electrodes formed on the silicon substrate.

Figure 2 shows the microfluidic channel made by PDMS which was installed on 32 G-FETs. The PBS solution is introduced from the right-hand side inlet, passes over 32 G-FET channels, and finally drained out from the left-hand side outlet in order to exchange the buffer solution and also to wash away the physical adsorption of viruses. The flow rate and the flow time can be precisely controlled by the computer controlled micro-pump. Using the microfluidic channel, the exchange of the PBS solution and the washing of the physical adsorption of the virus becomes possible for the precise detection of the virus.

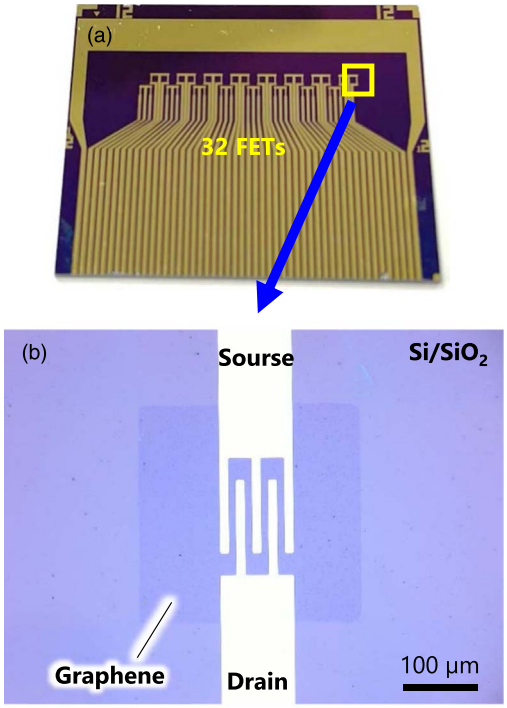

Fig. 1. (a) Optical image of integrated 32 G-FET. (b) Optical image of expanded view of one G-FET.

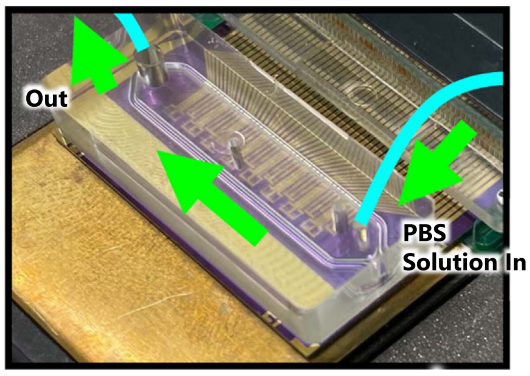

Fig. 2. Microfluidic channel installed on 32 G-FETs.

To enhance the sensitivity of G-FET, PLL was used to modulate the ζ potential of graphene. The Grahame equation which shows the relationship between the surface potential and the surface charge is shown below.[16)]

$$\sigma = \sqrt{8k_{\mathrm{B}}T\varepsilon\varepsilon_0 c_0}\,\sinh\left(\frac{zq\Psi_0}{2k_{\mathrm{B}}T}\right) \tag{1}$$

Where σ is the charge density of a unit area, k_{B} is the Boltzmann constant, ε is a relative permittivity, ε_0 is the permittivity of the vacuum, c_0 is the bulk ionic strength, z is the valency of the electrolyte, q is the elementary charge, Ψ_0 is surface potential.

The total concentration of NaCl and KCl which are monovalent ions in 1 × PBS is about 140 mM. On the other hand, the total concentration of KH_2PO_4 and Na_2HPO_4 which are multivalent ions in 1 × PBS is about 10 mM. The concentration of these multivalent ions is much smaller than that of monovalent ions. Thus, the effect of these multivalent ions could be ignored in this paper. From the Grahame Eq. (1), the sensitivity considering the concentration of electrolyte and the pH can be approximated as[17)]

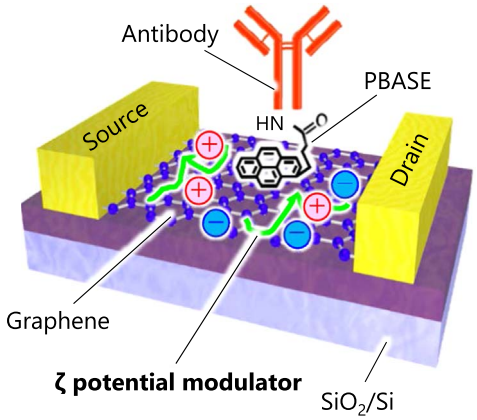

Fig. 3. Schematic structure of G-FET modified with antibody and ζ potential modulator.

$$\frac{d\Psi_0}{d\sigma_{ana}} \sim \frac{1}{\cosh\left(\frac{zq\Psi_0}{2k_{\mathrm{B}}T}\right)} \tag{2}$$

From this Eq. (2), the sensitivity could be maximized when $\cosh\left(\frac{zq\Psi_0}{2k_{\mathrm{B}}T}\right)$ becomes near 1, i.e. Ψ_0 becomes near 0 and/or the surface charge calculated from Eq. (1) becomes near 0.

Figure 3 shows the schematic structure of G-FET for the biosensing. The surface of G-FET was modified by SARS-CoV-2 spike antibody or Influenza H10N8 Hemagglutinin antibody via 1-Pyrenebutyric acid N-hydroxy-succinimide ester (PBASE).[24–27)] Graphene and PBASE which is dissolved in 2-methoxyethanol bound by π stacking. PBASE and the antibody which is dissolved in 0.2 × PBS bound by amide bond. In order to enhance the sensitivity of G-FET biosensor, the negative charge at the graphene surface should be canceled out and the surface charge of graphene should be as small as possible. For this purpose, the ζ potential modulator, which is a kind of cation polymer was added to G-FET.

In order to compare the effects of the ζ potential modulator, 4 kinds of G-FETs were prepared as shown in Fig. 4. Also, in order to solve the effect of the physical adsorption of the virus and of the drift,[28,29)] the reference FETs were prepared. Two G-FETs were modified by SARS-CoV-2 spike antibody with [Area (i)] and without [Area (ii)] the ζ potential modulator. The other two G-FETs were modified by Influenza H10N8 Hemagglutinin antibody with [Area (iii)] and without [Area (iv)] the ζ potential modulator. 32 integrated G-FETs are divided into 4 areas as shown in Fig. 4 by the silicon lubber pool. Each area is modified as follows:

(i) Area of FETs modified with SARS-CoV-2 spike antibody and the ζ potential modulator.
(ii) Area of FETs modified with SARS-CoV-2 spike antibody.
(iii) Area of FETs modified with Influenza H10N8 Hemagglutinin antibody and the ζ potential modulator.
(iv) Area of FETs modified with Influenza H10N8 Hemagglutinin antibody.

(iii) and (iv) were used as the reference FETs to remove the effect of physical adsorption of the viral charge and the drift.

Figure 5 shows the transfer characteristics of G-FET of area (i) in Fig. 4 before and after the introduction of the ζ

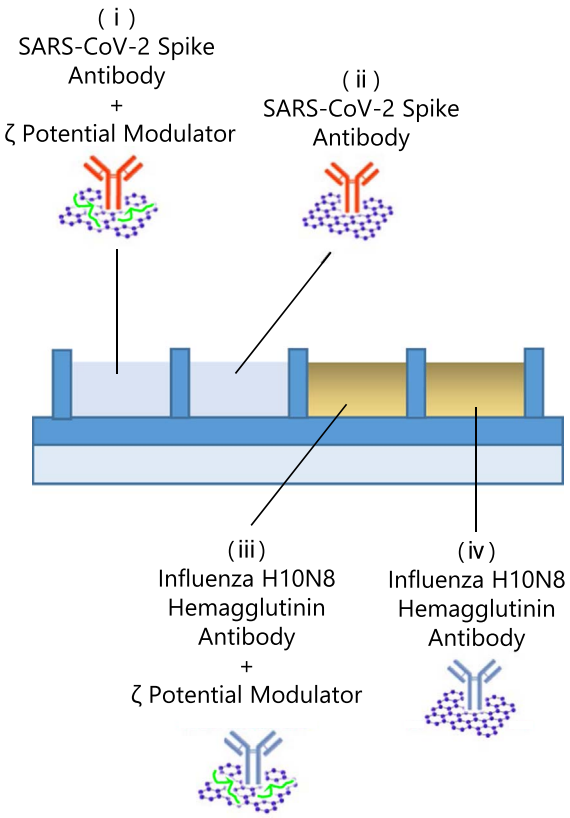

Fig. 4. 4 kinds of G-FET were prepared on same substrate in order to compare effects of ζ potential modulator, and also to cancel out problems of physical adsorption of virus and of drift.

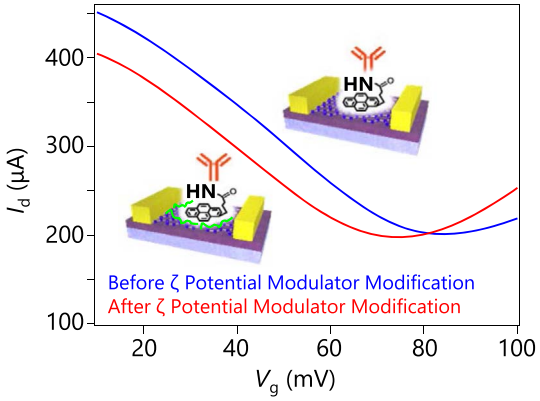

Fig. 5. Transfer characteristics of G-FET modified with SARS-CoV-2 spike antibody before and after introduction of ζ potential modulator.

potential modulator. The ζ potential modulator was introduced into G-FET after modifying SARS-CoV-2 spike antibody. The horizontal axis is the gate voltage V_G and the vertical axis is the drain current I_D. In this experiment, the source/drain voltage V_{SD} was fixed at 100 mV and V_G was swept between 0 and 500 mV. The gate voltage was applied to G-FET channel through the PBS solution, using the reference electrode as the gate electrode. The filtering process was not applied to the obtained transfer characteristics. To reduce the noise, the Dirac Point was calculated by polynomial fitting of the transfer characteristics. The actual measurement was performed by the portable measurement system fabricated by Murata Manufacturing Co., Ltd. with the performance equivalent to a conventional parameter analyzer. The Dirac point was measured by applying the top gate voltage when the microfluidic channel was filled with 0.01 × PBS. The blue line is the transfer characteristics before the introduction of the ζ potential modulator, and the red line after the introduction of the ζ potential modulator. In Fig. 5, the Dirac point of G-FET shifted in the negative direction after the introduction of the ζ potential modulator. This shift was caused by the positive charge of the ζ potential modulator which induce the negative charge in G-FET. Thus, we could confirm that the ζ potential modulator was successfully introduced onto the graphene surface by this shift.

3. Results and discussion

In order to confirm the enhancement effect of the sensitivity of G-FET by the introduction of the ζ potential modulator, the sensitivity of G-FET with and without the ζ potential modulator was compared as shown in Fig. 6. Figure 6 shows the result of the detection of the inactivated SARS-CoV-2[30] using G-FET modified by SARS-CoV-2 spike antibody with [Area (i) in Fig. 4] and without [Area (ii) in Fig. 4] the ζ potential modulator. The blocking of G-FET was performed using 0.01% Polyoxyethylene Sorbitan Monolaurate (Tween 20) before this measurement. The horizontal axis is the time and the vertical axis is the difference of the Dirac point (Δ Dirac point). This graph is the calculated result by subtracting the average of the Dirac point of G-FET without the ζ potential modulator [Area (ii) in Fig. 4] from that with the ζ potential modulator [Area (i) in Fig. 4] in order to remove the effect of the physical adsorption of the virus and the drift. It is necessary to use the high salt concentration of as high as 1 × PBS (150 mM) when SARS-CoV-2 bind well to the antibody.[31] Although PBS is essential for handling biological samples, the Debye length will not be as simple as the conventional formula of Debye length due to the presence of multiply charged ions. However, assuming that the Debye length is about 1 nm[32] in 150 mM PBS, it is shorter than the size of the antibody.[33,34] It is reasonable that the Debye length in 1.5 mM PBS is about 10 times longer according to the Debye length formula.[35,36] The 1 × PBS used in this experiment was purchased from Nacalai Tesque, Inc. and 0.01 × PBS was made by diluting PBS 100 times with pure water. In Fig. 6, the measurement of the Dirac point starts with the low salt concentration of 0.01 × PBS【1】. Then, the high salt concentration of 1 × PBS without SARS-CoV-2 was introduced two times【2】【4】to the system to check whether there were no disturbance by the exchange of the solution. Then, 1 × 10^6 FFU ml^{-1}【6】and 1 × 10^7 FFU ml^{-1}【8】SARS-CoV-2 in 1 × PBS were introduced into the system and the Dirac point shift was measured. If the viral charge enters within the Debye length, G-FET can detect the negative charge of the SARS-CoV-2 virus[37] and the Dirac point shifts toward the positive direction. After the virus bound to the antibody sufficiently, 0.01 × PBS was, then, introduced to the microfluidic channel to wash away the free-floating virus in the solution and the physical adsorption of viruses on graphene, so that only the charge of the virus specifically bound to the antibody was detected【7】【9】. Before and after the exchange of the solution without SARS-CoV-2, i.e. the area【1】【3】【5】, the Dirac point shift

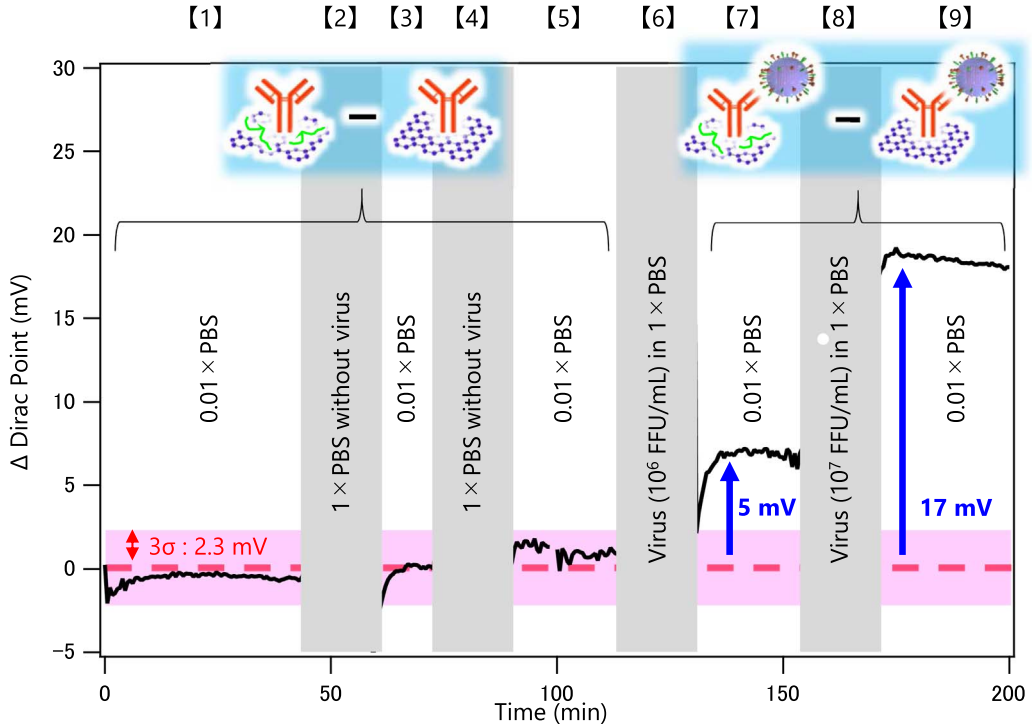

Fig. 6. Result of detection of SARS-CoV-2 using G-FET modified by SARS-CoV-2 spike antibody with and without ζ potential modulator. Graph is calculated result by subtracting average of Dirac point shift of G-FET without ζ potential modulator from that with ζ potential modulator.

shows only small increase. The average of these Dirac point shifts is shown by the red dashed line in Fig. 6. The three times of the standard deviation, 3σ of the Dirac point shift in these areas of 【1】 【3】 【5】 is 2.3 mV, and is shown in the pink shadow. After the introduction of SARS-CoV-2 with the concentration of 1×10^6 FFU ml^{-1} 【6】 and 1×10^7 FFU ml^{-1} 【8】, the large Dirac point shifts of 5 mV and 17 mV were observed, respectively. Because these values are beyond 3σ (2.3 mV), it is said that this response is due to the negative charge of SARS-CoV-2. Thus, these results imply that the sensitivity of G-FET was improved by applying the ζ potential modulator.

Figure 7 shows the experimental result of the detection of SARS-CoV-2 by using G-FET modified with SARS-CoV-2 spike antibody and also with the ζ potential modulator [Area (i) in Fig. 4]. G-FET modified with Influenza H10N8 Hemagglutinin antibody with the ζ potential modulator [Area (iii) in Fig. 4] was used as the reference FETs in order to remove the effect of the physical adsorption of the viral charge and the drift effect. The graph in Fig. 7 is the calculated results by subtracting the average of the Dirac point of G-FET modified with Influenza H10N8 Hemagglutinin antibody and the ζ potential modulator [Area (iii) in Fig. 4] from that with SARS-CoV-2 spike antibody and the ζ potential modulator [Area (i) in Fig. 4]. The horizontal axis is the time and the vertical axis is the difference of Dirac point. Two times of 1 × PBS without the virus 【11】 【13】 and two kinds of concentration of SARS-CoV-2 in 1 × PBS 【15】 【17】 were introduced into the system. Subsequently, 0.01 × PBS was introduced into the system 【16】 【18】 to extend the Debye length about ten times for the detection of the viral charge as a shift of the Dirac point. Before and after the exchange of the solution without SARS-CoV-2, i.e. the area 【10】 【12】 【14】, the Dirac point shift shows only small increase, and the average of these Dirac point shifts is shown by the red dashed line in Fig. 7. Also, 3σ of the Dirac point shift in these areas of 【10】 【12】 【14】 is 4.9 mV, and is shown in the pink shadow. After the introduction of SARS-CoV-2 with the concentration of 1×10^6 FFU ml^{-1}, Δ Dirac point was as small as ∼1.3 mV 【16】 and it does not exceed 3σ and is considered to be under the noise level. After the introduction of SARS-CoV-2 with the concentration of 1×10^7 FFU ml^{-1}, however, Δ Dirac point was as large as 10 mV 【18】 and it exceeds the 3σ. Therefore, it can be said that this response is originated from the negative charge of SARS-CoV-2 binding to the antibody, selectively.

In order to confirm the enhancement effect of the ζ potential modulator, G-FET "without the ζ potential modulator" was used to detect SARS-CoV-2. Figure 8 shows the experimental result of the detection of SARS-CoV-2 by using G-FET modified with SARS-CoV-2 spike antibody "without the ζ potential modulator" [Area (ii) in Fig. 4]. G-FET modified with Influenza H10N8 Hemagglutinin antibody "without the ζ potential modulator" [Area (iv) in Fig. 4] was used as the reference FETs. Figure 8 is the calculated results by subtracting the average of the Dirac point of G-FET modified with Influenza H10N8 Hemagglutinin antibody "without the ζ potential modulator" [Area (iv) in Fig. 4] from that with SARS-CoV-2 spike antibody "without the ζ potential modulator" [Area (ii) in Fig. 4]. The horizontal axis is the time and the vertical axis is the difference of Dirac point. Two times of 1 × PBS without virus 【20】 【22】 and two kinds of concentration of SARS-CoV-2 in 1 × PBS 【24】 【26】 were introduced into the system. Subsequently, 0.01 × PBS was introduced into the system to extend the Debye length about ten times for the detection of the viral charge 【25】 【27】 as a shift of the Dirac point. Before and after the

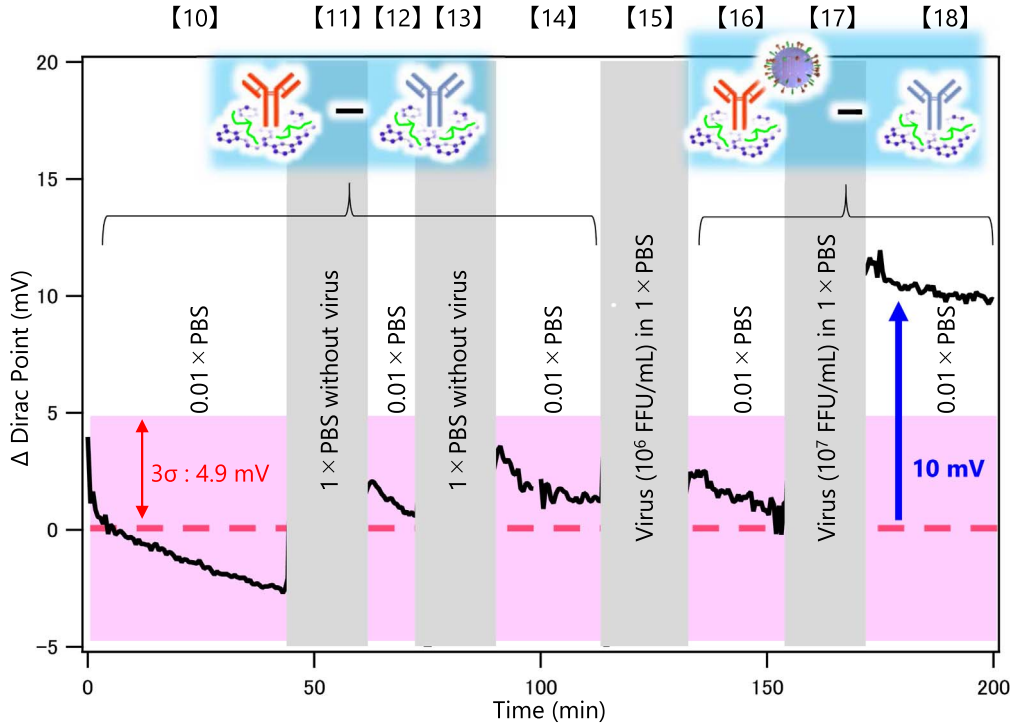

Fig. 7. Result of detection of SARS-CoV-2 using G-FET modified by SARS-CoV-2 spike antibody and by Influenza H10N8 Hemagglutinin antibody. Both FETs are modified by ζ potential modulator. Graph is calculated result by subtracting average of Dirac point shift of G-FET modified by Influenza H10N8 Hemagglutinin antibody from that by SARS-CoV-2 spike antibody.

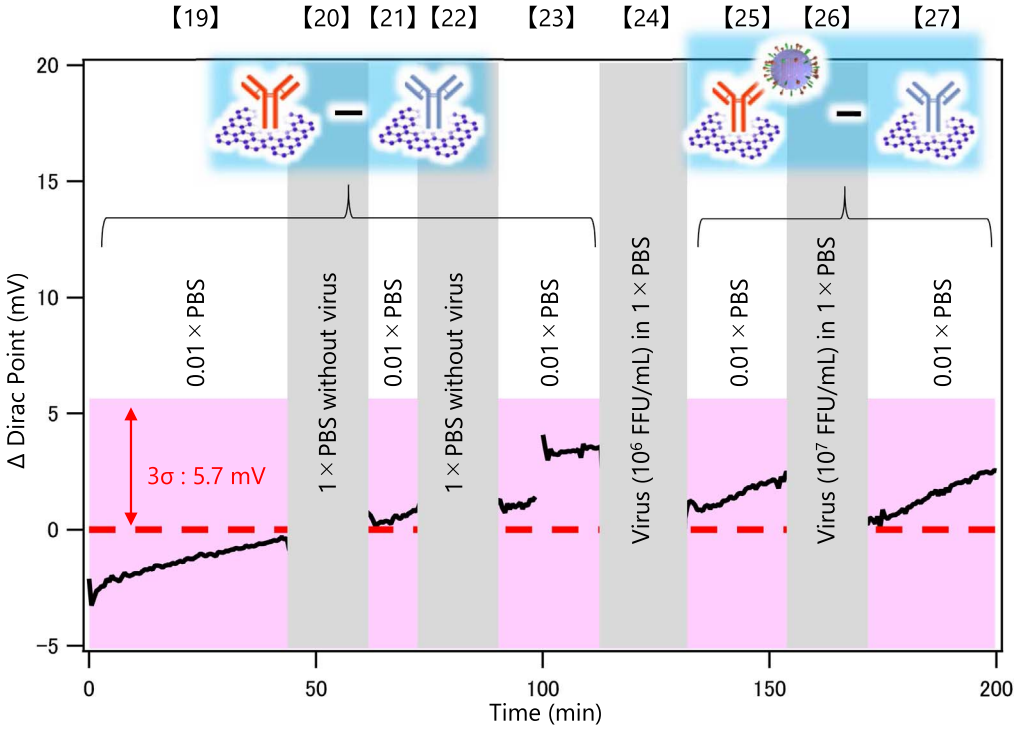

Fig. 8. Result of detection of SARS-CoV-2 using G-FET modified by SARS-CoV-2 spike antibody and by Influenza H10N8 Hemagglutinin antibody. Both FETs are NOT modified by ζ potential modulator. Graph is calculated result by subtracting average of Dirac point shift of G-FET modified by Influenza H10N8 Hemagglutinin antibody from that by SARS-CoV-2 spike antibody.

exchange of the solution without SARS-CoV-2, i.e. the area 【19】 【21】 【23】, the Dirac point shift shows only small increase, and the average of these Dirac point shifts is shown by the red dashed line in Fig. 8. Also, 3σ of the Dirac point shift in these areas of 【19】 【21】 【23】 is 5.7 mV, and is shown in the pink shadow. After the introduction of SARS-CoV-2 with the concentration of 1×10^6 FFU ml^{-1}, and 1×10^7 FFU ml^{-1} , Δ Dirac point does not exceed 3σ and is considered to be under the noise level 【25】 【27】. Comparing Fig. 6 with Figs. 7 and 8, the larger 3σ in Figs. 8(a) and 9 is considered to be due to the difference in the drift between G-FETs. Figure 6 is the result of subtracting the Dirac Points of G-FETs modified with the same type of antibody from each other, while Figs. 7 and 8 are the results of

subtracting the Dirac Points of G-FETs modified with the different types of antibodies. The different antibodies are thought to be responsible for the larger drifts in Figs. 7 and 8 compared to Fig. 6. The different environments on graphene often cause different properties such as drift.

Using the ζ potential modulator as shown in Fig. 7, SARS-CoV-2 with the concentration of 1×10^7 FFU ml^{-1} was clearly detected 【18】, but without the ζ potential modulator as shown in Fig. 8, SARS-CoV-2 with the same concentration of 1×10^7 FFU ml^{-1} could not be detected 【27】. These results clearly show the enhancement of the sensitivity using the ζ potential modulator.

4. Conclusions

Using G-FET modified with SARS-CoV-2 spike antibody and the ζ potential modulator, SARS-CoV-2 could be detected. By applying the ζ potential modulator on G-FET biosensor, we have succeeded in the great enhancement of the sensitivity of G-FET. And also, the effect of the physical adsorption of the viral charge and of the drift could be removed by using the reference FETs modified with Influenza H10N8 Hemagglutinin antibody. Thus, only the charge of the virus selectively binding to the antibody could be precisely detected.

Acknowledgments

This study was supported by the JST-Mirai project (JPMJMI22D2) and the JST CREST project (JPMJCR15F4).

ORCID iDs

Takao Ono https://orcid.org/0000-0002-6717-123X
Yasushi Kanai https://orcid.org/0000-0002-6501-9699
Shota Ushiba https://orcid.org/0000-0001-7652-081X

1) E. H. Hwang, S. Adam, and S. Das Sarma, Phys. Rev. Lett. **98**, 186806 (2007).
2) K. I. Bolotin, K. J. Sikes, Z. Jiang, M. Klima, G. Fudenberg, J. Hone, P. Kim, and H. L. Stormer, Solid State Commun. **146**, 351 (2008).
3) J. Liu, J. Tang, and J. J. Gooding, J. Mater. Chem. **22**, 12435 (2012).
4) T. Kawata, T. Ono, Y. Kanai, Y. Ohno, K. Maehashi, K. Inoue, and K. Matsumoto, Jpn. J. Appl. Phys. **57**, 065103 (2018).
5) Y. Ohno, K. Maehashi, Y. Yamashiro, and K. Matsumoto, Nano Lett. **9**, 3318 (2009).
6) M. Shimatani, S. Ogawa, D. Fujisawa, S. Okuda, Y. Kanai, T. Ono, and K. Matsumoto, AIP Adv. **6**, 035113 (2016).
7) S. Ushiba, T. Ono, Y. Kanai, K. Inoue, M. Kimura, and K. Matsumoto, ACS Omega **3**, 3137 (2018).
8) S. Ushiba et al., Appl. Phys. Exp. **14**, 036504 (2021).
9) S. Ushiba, T. Nakano, N. Miyakawa, A. Shinagawa, T. Ono, Y. Kanai, S. Tani, M. Kimura, and K. Matsumoto, Appl. Phys. Exp. **15**, 115002 (2022).
10) Y. Ohno, K. Maehashi, and K. Matsumoto, J. Am. Chem. Soc. **132**, 18012 (2010).
11) Y. Kanai, M. T. Y. Ohmuro-Matsuyama, T. K. S. Ushiba, T. Ono, K. Inoue, M. Kimura, H. Ueda, and K. Matsumoto, ACS Sens. **5**, 24 (2020).
12) T. Ono et al., Jpn. J. Appl. Phys. **56**, 030302 (2017).
13) T. Ono, Y. Kanai, K. Inoue, Y. Watanabe, S. Nakakita, T. Kawahara, Y. Suzuki, and K. Matsumoto, Nano Lett. **19**, 4004 (2019).
14) S. Ushiba et al., ACS Omega **8**, 49270 (2023).
15) K. S. Novoselov, A. K. Geim, S. V. Morozov, D. Jiang, M. I. Katsnelson, I. V. Grigorieva, S. V. Dubonos, and A. A. Firsov, Nature **438**, 197 (2005).
16) M. Gupta, S. Santermans, G. Hellings, L. Lagae, K. Martens, and W. Van Roy, IEEE Sens. J. **21**, 4143 (2021).
17) B. K. Wunderlich, P. A. Neff, and A. R. Bausch, Appl. Phys. Lett. **91**, 083904 (2007).
18) G. Bepete, E. Anglaret, L. Ortolani, V. Morandi, K. Huang, A. Pénicaud, and C. Drummond, Nat. Chem. **9**, 347 (2017).
19) K. Yamamoto et al., Ext. Abst. Solid State Devices and Materials 2023, p. 797.
20) E. Piccinini, G. E. Fenoy, A. L. Cantillo, J. A. Allegretto, J. Scotto, J. M. Piccinini, W. A. Marmisollé, and O. Azzaroni, Adv. Mater. Interfaces **9**, 2102526 (2022).
21) A. Silvestri et al., Nanoscale **15**, 1076 (2022).
22) M. Taeyoung Hwang, I. Park, M. Heiranian, A. Taqieddin, S. You, V. Faramarzi, A. A. Pak, A. M. Van Der Zande, N. R. Aluru, and R. Bashir, Adv. Mater. Technol. **6**, 2100712 (2021).
23) I. Park et al., ACS Sens. **6**, 4461 (2021).
24) L. Zhou et al., Biosens. Bioelectron. **87**, 701 (2017).
25) M. A. Ehsan, S. A. Khan, and A. Rehman, Diagnostics **11**, 1030 (2021).
26) D. K. Hong Tsang, T. J. Lieberthal, C. Watts, I. E. Dunlop, S. Ramadan, A. E. del Rio Hernandez, and N. Klein, Sci. Rep. **9**, 13946 (2019).
27) J. W. Kim, S. Kim, Y-ha Jang, K-il Lim, and W. H. Lee, Nanotechnology **30**, 345502 (2019).
28) S. Ushiba, T. Okino, N. Miyakawa, T. Ono, A. Shinagawa, Y. Kanai, K. Inoue, K. Takahashi, M. Kimura, and K. Matsumoto, Jpn. J. Appl. Phys. **59**, SGGH04 (2020).
29) N. Miyakawa, A. Shinagawa, Y. Kajiwara, S. Ushiba, T. Ono, Y. Kanai, S. Tani, M. Kimura, and K. Matsumoto, Sensors **21**, 7455 (2021).
30) C. Kandiyil, P. Jendrny, F. Twele, V. Pilchov, A. Volk, A. Osterhaus, and M. Von K, J. Virol. Methods **317**, 114733 (2023).
31) A. Silva De Souza, J. D. Rivera, V. M. Almeida, P. Ge, R. F. De Souza, C. S. Farah, H. Ulrich, S. R. Marana, R. K. Salinas, and C. R. Guzzo, J. Phys. Chem. Lett. **11**, 10446 (2020).
32) R. Elnathan, M. Kwiat, A. Pevzner, Y. Engel, L. Burstein, A. Khatchtourints, A. Lichtenstein, R. Kantaev, and F. Patolsky, Nano Lett. **12**, 5245 (2012).
33) J. W. Jay, B. Bray, Y. Qi, E. Igbinigie, and H. Wu, Antibodies **7**, 18 (2018).
34) Y. Oka, S. Ushiba, N. Miyakawa, M. Nishio, T. Ono, Y. Kanai, Y. Watanabe, S. Tani, M. Kimura, and K. Matsumoto, Biophys. Physicobiol. **19**, e190003 (2022).
35) E. Stern, R. Wagner, F. J. Sigworth, R. Breaker, T. M. Fahmy, and M. A. Reed, Nano Lett. **7**, 3405 (2007).
36) J. N. Israelachvili, 1985)*Intermolecular and Surface Forces: With Applications to Colloidal and Biological Systems* (Academic, London).
37) O. Areo, P. U. Joshi, M. Obrenovich, M. Tayahi, and C. L. Heldt, Microorganisms **9**, 3 (2021).